


Giant Two-Level Systems in a Granular Superconductor

M. Kristen^{1,2}, J. N. Voss,² M. Wildermuth², A. Bilmes,² J. Lisenfeld², H. Rotzinger^{1,2,*} and A. V. Ustinov^{1,2}

¹*Institute for Quantum Materials and Technology, Karlsruhe Institute of Technology, 76131 Karlsruhe, Germany*

²*Physikalisches Institut, Karlsruhe Institute of Technology, 76131 Karlsruhe, Germany*

 (Received 18 July 2023; revised 9 February 2024; accepted 11 February 2024; published 22 May 2024)

Disordered thin films are a common choice of material for superconducting, high impedance circuits used in quantum information or particle detector physics. A wide selection of materials with different levels of granularity are available, but, despite low microwave losses being reported for some, the high degree of disorder always implies the presence of intrinsic defects. Prominently, quantum circuits are prone to interact with two-level systems (TLS), typically originating from solid state defects in the dielectric parts of the circuit, like surface oxides or tunneling barriers. We present an experimental investigation of TLS in granular aluminum thin films under applied mechanical strain and electric fields. The analysis reveals a class of strongly coupled TLS having electric dipole moments up to $30 e\text{\AA}$, an order of magnitude larger than dipole moments commonly reported for solid state defects. Notably, these large dipole moments appear more often in films with a higher resistivity. Our observations shed new light on granular superconductors and may have implications for their usage as a quantum circuit material.

DOI: [10.1103/PhysRevLett.132.217002](https://doi.org/10.1103/PhysRevLett.132.217002)

Originally studied with regard to their enhanced critical temperature [1], thin films of disordered superconductors have regained popularity in recent years due to their outstanding high frequency properties, which stem mainly from their low intrinsic charge carrier density [2]. In these materials, the large kinetic inductance can lead to circuit impedances in the $k\Omega$ range. This property has proven valuable for many applications, like single photon detectors [3–5], superconducting qubits [6–8], nanowire devices [9,10], and high impedance resonators [11–15].

The disordered structure of the material also favors the presence of defects throughout the entire film. In particular, defects forming coherent two-level systems (TLS) are known to exist in the amorphous surface oxides of superconducting films. Via their electric dipole moment, such TLS can couple to the ac fields of quantum circuits, causing energy relaxation and dephasing [16]. As a consequence, increasing experimental effort has been undertaken to investigate TLS origin, nature, and location. Individual TLS can be observed in superconducting qubits [17–22] and resonators [23,24], the latter being also used to study TLS ensembles in different materials [25–29].

In this Letter, we report on experiments with compact microwave resonators fabricated from granular aluminum thin films. The material consists of pure aluminum grains

with a diameter of about 4 nm embedded in a matrix of amorphous aluminum oxide, which self-assembles during the deposition of aluminum in an oxygen atmosphere [30]. In the growth process, the oxygen partial pressure influences the thickness of the oxide barrier separating the grains, typically 1–2 nm, and thus the normal state sheet resistance R_n [31]. If R_n is well below the resistance quantum $R_q = 6.45 k\Omega$, granular aluminum is superconducting ($T_c \sim 1.8$ K) and shows, compared to pure aluminum, a reduced charge carrier density as well as a sizeable kinetic sheet inductance $L_{kin} = 0.18\hbar R_n / (k_B T_c)$ in the nH/\square range.

For this study, we have patterned five different films (chips A–E, see Table I for details) into a total of thirteen $\lambda/2$ microstrip resonators. Depending on the sheet inductance, the resonator length was varied up to 500 μm at a constant width of 2 μm . On chip D and E, the resonators were covered by an additional, insulating layer of granular aluminum ($R_n \gg R_q$), in order to compare the contributions of different film surfaces to the dielectric loss.

Figure 1(a) provides a sketch of the experimental setup. We apply mechanical strain ξ_z using a voltage controlled piezoactuator up to $U_{piezo} = 40$ V ([18]) and electric fields up to $E_z = 629$ kV/m through parallel capacitor plates [32]. Here, $E_z(U_{elec})$ is the maximum field value along the resonator film edge (see Supplemental Material IV for technical details [33]). To monitor the resonance behavior, the microwave transmission S_{21} of the samples is recorded with a vector network analyzer in a millikelvin temperature setup.

For low applied microwave power (few photon regime), the transmission spectrum reveals numerous anti-crossings

Published by the American Physical Society under the terms of the [Creative Commons Attribution 4.0 International license](https://creativecommons.org/licenses/by/4.0/). Further distribution of this work must maintain attribution to the author(s) and the published article's title, journal citation, and DOI.

TABLE I. Overview of the characteristic sample parameters. Each chip hosts several resonators with similar geometry and sheet resistance R_n .

Chip	A	B	C	D ^a	E ^a
Thickness (nm)	25	22	30	24 + 17	23 + 17
R_n (k Ω /□)	0.6	1.5	4.1	0.7 + 12	0.7 + 190
No. Resonators	2	3	3	3	2

^aSample is fabricated from a bilayer, which consists of a superconducting (bottom) and insulating (top) granular aluminum film.

over a wide range of electric fields, see Fig. 1(b) for a subset of the data [strain: Fig. 1(c)]. In the vicinity of an anticrossing, the resonance frequency ω_r shifts and the linewidth κ increases noticeably, as illustrated by the inset of Fig. 1(b). A sweep of the power P_{MW} , see Fig. 2(a), suggests a dependence of this resonance broadening on the average resonator photon number $\bar{n} \propto P_{MW}/(\hbar\omega_r^2)$ [38]. At low photon numbers (blue line), two pronounced peaks in the relative linewidth κ/κ_0 clearly indicate an anticrossing. This feature gradually gets washed out as \bar{n} increases and disappears around $\bar{n} = 10^4$ (red line). Subsequently, we monitored the increased linewidth over a two-day period in a wider range of electric fields [Fig. 2(b)]. There, the electric field values E_z^i , at which the anticrossings occur, fluctuate noticeably. We identify a telegraphiclike switching pattern between two E_z^i values as well as sudden jumps to a different E_z^i .

Overall, the strain and electric field experiments show a similar qualitative picture [see Figs. 1(b) and 1(c)]. However, strain measurements are inconsistent due to the hysteretic nature of the piezoactuator, which makes a direct comparison of the data difficult. In the following, we therefore focus on experiments with electric fields, which also show a higher anticrossing count.

Under the assumption that the measured anticrossings stem from the coherent interaction of the resonator with TLS [16], the experimental data can be separated into two classes: (i) strongly coupled TLS characterized by a coupling strength $g \approx \kappa$ on the order of the resonator linewidth and (ii) moderately coupled TLS with $g \ll \kappa$. While the TLS type (i) generates more pronounced anticrossings, the TLS of type (ii) actually make up most of the total anticrossings count (see Supplemental Material III for the detailed statistics [33]).

Because of their typically low lifetimes [20,21,32,39], near resonant TLS present a very effective loss channel for superconducting resonators. Since a single TLS can only absorb one photon at a time, the loss is expected to saturate when the number of available photons \bar{n} is large enough such that the TLS are, on average, already excited. This behavior can be seen in Fig. 2(a). The telegraphic switching as well as the sudden jumps of the resonator frequency [Fig. 2(b)] are also known signatures of TLS dynamics [27,40–42]. Such fluctuations are generally attributed to the coupling of a resonant TLS to secondary TLS at much lower frequencies ($\hbar\omega_{TLS} \leq k_B T$), undergoing incoherent tunneling or random thermal transitions [43]. The collective behavior of the anticrossing pair around $E_z^i = 40$ kV/m indicates that it belongs to a single TLS.

An evaluation of data from all resonators yields an average density of 1/30 GHz for all observable TLS. An independent analysis of the resonator loss tangent $\tan(\delta_0) \propto \kappa(\bar{n} \rightarrow 0)$, however, suggests that these TLS are not solely responsible for the entire dielectric loss, which is more likely to be dominated by a bath of weakly coupled TLS which are not directly observable in our measurements (for details, see Supplemental Material VI [33]).

The quantum mechanical model of a TLS (a tunneling particle in an asymmetric double well potential [44,45]), yields a transition frequency

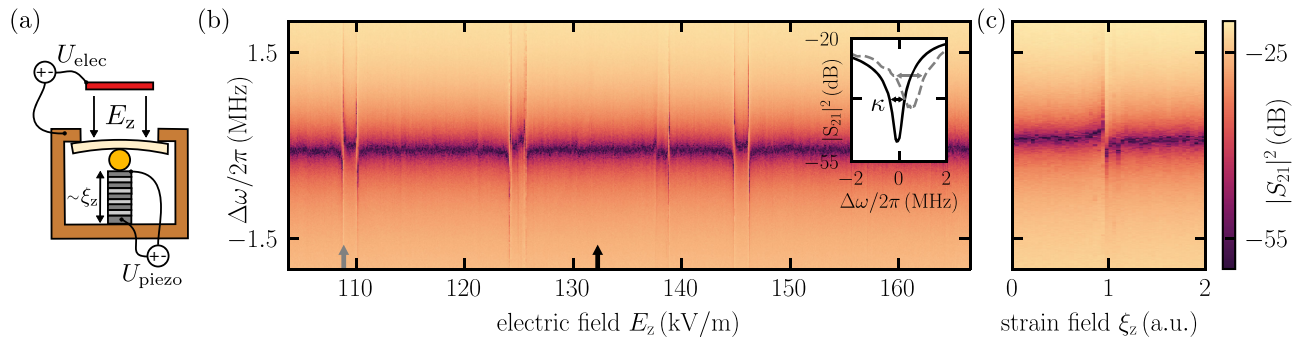


FIG. 1. Resonator measurements with applied mechanical strain and electric fields. (a) Sketch of the sample holder. A piezoactuator and a dc electrode are used to manipulate the strain ξ and the electric field \vec{E} . (b) Sample transmission amplitude $|S_{21}|^2$ in a spectral window $\Delta\omega = \omega - \omega_r$ around the resonance frequency at $\omega_r = 7.84$ GHz, as a function of the maximum electric field at the film surface E_z . The inset illustrates how the linewidth κ of the unperturbed resonance (black) increases near one of the anticrossings (gray). Inset data is smoothed for visibility. (c) Resonator transmission as a function of mechanical strain applied to the film.

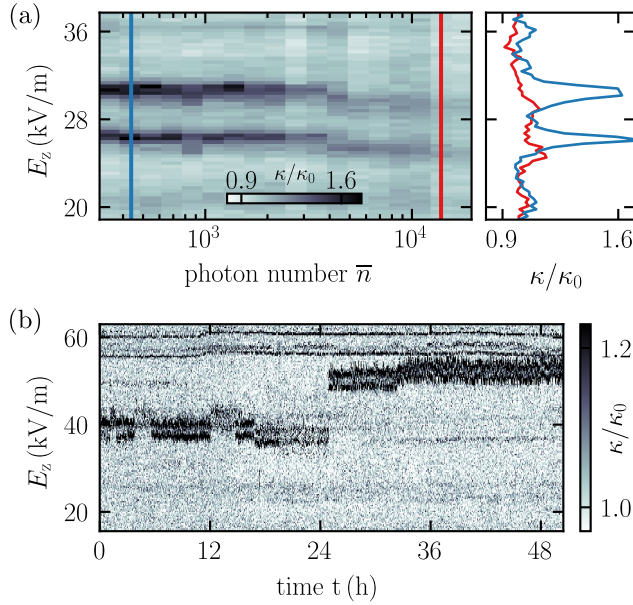


FIG. 2. Resonator loss traces. (a) Relative resonator linewidth κ/κ_0 as a function of the electric field and the average photon number \bar{n} . Near an anticrossing, κ is noticeably increased (darker color). The anticrossings get washed out as the photon number increases $\bar{n} \rightarrow 10^4$. (b) Tracing several anticrossings over a two-day period. The data reveal various types of temporal fluctuations.

$$\omega_{\text{TLS}} = \frac{1}{\hbar} \sqrt{\Delta^2 + (\epsilon + 2d|E_z| + 2\gamma^* \xi_z)^2}. \quad (1)$$

Here, Δ and ϵ are the tunneling and asymmetry energies of the unperturbed TLS, γ^* is the effective coupling strength to the strain field $\xi_z = |\vec{\xi}|$ and d is the component of the TLS's electric dipole moment that is parallel to the maximum expected field strength E_z . Therefore, d is a lower bound for the TLS dipole moment $|\vec{d}|$. Because of the quadratic terms in Eq. (1) there are always two E_z^{ac} values where the frequencies of TLS and resonator cross ($\omega_{\text{TLS}} = \omega_r$), provided that $\Delta < \hbar\omega_r$. For moderately coupled TLS with $\Delta \approx \hbar\omega_r$, a hyperbolic trace in accordance with Eq. (1) is, on rare occasions, visible in the transmission spectrum over the whole frequency range $\Delta\omega$ (see Supplemental Material II for additional measurement data [33]).

We now take a closer look at the pronounced anticrossings in our spectra. Following Sarabi *et al.* [23], the Jaynes-Cummings model for a resonator and a single, strongly coupled TLS yields an analytical expression for the microwave transmission in the vicinity of an anticrossing

$$S_{21} \propto 1 - \frac{\bar{\kappa}_c/2}{\kappa/2 + i(\omega - \omega_r) + g^2[\gamma_{\text{TLS}}/2 + i(\omega - \omega_{\text{TLS}})]^{-1}}. \quad (2)$$

Here, κ and γ_{TLS} are the linewidths of resonator and TLS. The external loss rate of the resonator $\bar{\kappa}_c$ has a complex

component due to the nonideal transmission line [46]. We use Eq. (2) together with Eq. (1) to fit the model to the measured transmission data in the vicinity of anticrossings with strongly coupled TLS. In particular, only symmetric anticrossing pairs were selected [top inset Fig. 3(b)], ensuring unambiguous values for the extracted parameters. On the basis of 86 analyzed anticrossings obtained in two independent measurement runs, we find a wide distribution of TLS linewidths ranging from 0.2 to 80 MHz [Fig. 3(a)]. The average linewidth value $\bar{\gamma}_{\text{TLS}}/2\pi \approx 14$ MHz, corresponding to a coherence time of a few hundreds of nanoseconds, is comparable to values found in similar studies on superconducting qubits [32,39] and distributed microwave resonators [24,47].

The extracted values for the coupling strength g and dipole moment d are shown in Fig. 3(b). For reference, the hatched area indicates the estimated parameter space for conventional TLS originating, e.g., from atomic defects (AD), in agreement with earlier experiments that have reported dipoles $|d_{\text{AD}}|$ of up to $2 \text{ e}\text{\AA}$ [20,48–52]. While the TLS of type (ii) fall into this region, the analysis of the more pronounced anticrossings shows a different picture. Specifically, order of magnitude larger dipole moments, up to $30 \text{ e}\text{\AA}$, and coupling strength $g/2\pi > 1$ MHz are extracted from the fits. Both quantities are statistically correlated (Pearson correlation coefficient $r = 0.61$), as expected for $g \propto E_{\text{rms}}|\vec{d}|$. Here, $E_{\text{rms}} \propto \sqrt{Z_r}$ is the maximum single-mode resonator field at the film surface, which is enhanced by the high characteristic impedance of the resonator Z_r (see Supplemental Material IV for technical details [33]).

Interestingly, TLS with a coupling strength of $g/2\pi > 2$ MHz are only observed on samples *B* and *C*. This supports the assumption that for the two-layer samples (*D* and *E*), most strongly coupled TLS reside in the insulating top layer, while the resonator currents flow only in the lower, superconducting layer. Then, screening effects partially reduce E_{rms} for these TLS, while E_z remains comparable for all samples.

The bottom inset in Fig. 3(b) shows the density of strongly coupled TLS found in each sample, normalized to an electric field tuning range of one megavolt per meter. The values increase with R_n , also for the films with the insulating capping layer. In particular, the TLS density in sample *E* is noticeable higher than in sample *A*, despite an almost identical sheet resistance of the resonating layer.

Using atomic force microscopy, we measure a rather low surface roughness of $S_q \leq 1$ nm for the granular aluminum film, which is comparable with the surface roughness of pure aluminum $S_q \geq 1$ nm. This supports the assumption that the electric fields at the resonator film edge do not experience a substantial enhancement due to the granularity of the film. Consequently, the observation of dipole moments far exceeding $2 \text{ e}\text{\AA}$ points towards the existence

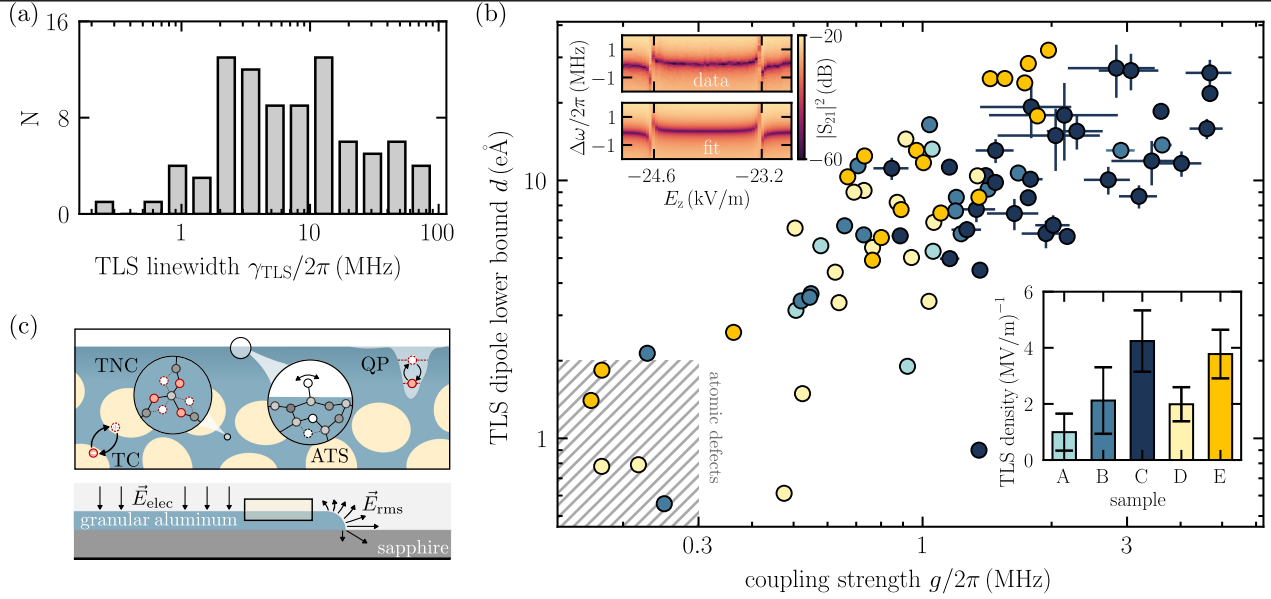


FIG. 3. Analysis of strongly coupled TLS. (a) Distribution of TLS linewidth γ_{TLS} obtained from 86 fits on data from all samples. (b) Resonator-TLS coupling strength g and TLS dipole d extracted from the same fits. Single layer samples are colored in shades of blue, two-layer samples in shades of yellow. Error bars smaller than the marker size are not shown. Hatched area indicates the parameter space expected for atomic defects. Top inset: Transmission spectrum of the resonator in the vicinity of a strongly coupled TLS. Bottom inset: Average number of strongly coupled TLS in one megavolt per meter electric field range, as found on each sample. Error bars indicate variations between different resonators and cooldowns. (c) Top: Sketch of the granular aluminum film surface, illustrating atomic defects (blue) as well as potential candidates with larger dipole moments (red). The latter includes charges trapped on or between grains, tunneling nanoclusters of atoms, or quasiparticles trapped due to spatial variations of the superconducting gap. Bottom: Side view of the sample showing the relevant electric fields (not to scale).

of TLS having a previously unknown microscopic origin. Possible candidates are illustrated in Fig. 3(c).

In a recent publication, dipole moments of similar size have been observed by studying the dielectric loss of amorphous silicon under a swept electric field [53]. The findings were interpreted in the scope of a two-TLS model [54]. There, TLS are classified, similar to this work, into a weakly and a strongly interacting variety, where the latter can have very large electric dipole moments but is generally only observed under nonequilibrium conditions. In the equilibrium case, phonon mediated TLS-TLS interactions create a gap in the energy spectrum at the relevant energies [55,56]. If, however, the sample is disordered, it has been shown that the granularity modifies the phonon spectrum [57], which might obstruct the TLS-TLS interaction and lift the gap.

For the above mechanism to be effective, such TLS have to sit at the grain boundaries rather than the surface oxide of the film. They could, for instance, be formed by tunneling nanoclusters (TNC) with up to hundreds of participating atoms [58]. For our study, the electrical field has to reach the TLS in order to modify its frequency. As a lower bound, we can roughly estimate the static field penetration depth $\lambda > \lambda_{\text{TF}} \simeq 2 \text{ nm}$ to be on the order of the Thomas-Fermi length (see Supplemental Material III for details [33]). Thus, since λ is comparable to the thickness of the films, we

can assume that the global field E_z does not only penetrate the surface oxide but also into the inner film parts, e.g., the oxide between the grains.

The prevalence of strongly coupled TLS in films with higher sheet resistance [inset Fig. 3(b)] suggests that the underlying physics might be related to the suppression of the global phase coherent state in these films [59], which is much more sensitive to changes in R_n than the film morphology. This assumption is supported by noise measurements performed earlier on these samples, where a dependence on R_n was also observed [60].

A potential TLS candidate that becomes more likely as the film resistance increases are quasiparticles (QP) localized due to spatial variations of the superconducting gap $\delta\Delta_{\text{sc}}$. This hypothesis has recently been reported as a novel type of TLS in disordered NbN films [61]. Such traps can arise, e.g., due to weak magnetic impurities or film inhomogeneities [62,63]. Compared to NbN, granular aluminum is characterized by an increased coherence length $\xi_{0,\text{grAl}} \approx 2\xi_{0,\text{NbN}}$. The consequence are wider ($\sim \xi_0^2$) traps and thus potentially larger dipoles, which are also shielded less efficiently due to the reduced charge carrier density. In granular aluminum, traps can also be expected to be shallower ($\delta\Delta_{\text{sc}} \approx 0.15\Delta_{\text{sc}} = 500 \text{ mK}$), resulting in a comparable distribution of TLS frequencies $\propto \Delta_{\text{sc}}\xi_0^2$ in both materials. We note that the highly resistive layers covering the

resonators on D and E might contain superconducting puddles where this effect can also occur [64–66].

Historically, a popular concept to explain strongly coupled TLS are tunneling charges (TC), for which evidence has been found in Josephson junctions [67,68] and Nb + Pt resonators [69]. In granular aluminum films, localized charges naturally occur when the sample approaches the superconductor to insulator transition (SIT) [64]. While the typical charging energy of fairly isolated grains on the order of several Kelvin does not match the presented findings, it has been shown that hopping charges can be dressed by phononic states of neighboring grains [70] or virtual tunneling processes [71], renormalizing the TLS energy.

The localization of charges near the SIT is accompanied by local fluctuations of the superconducting phase [72]. As a consequence, collective excitations of the condensate are expected to acquire dipole moments and appear as low-energy subgap features [73,74], which would be experimentally observable.

In conclusion, we have characterized two-level systems in oxidized granular aluminum films using electric field and strain tuning experiments. In addition to TLS with conventional properties, we observe a strongly coupled variety of TLS with orders of magnitude larger dipole moments. These TLS are found more frequently in samples with higher sheet resistances. Because of their pronounced frequency fluctuations and low lifetimes, they can be a severe source of noise and dissipation. Since the microscopic mechanism forming these large dipoles remains unknown, we are calling for additional experiments to uncover their nature. Possible pathways include lumped-element resonator geometries [23], which allow for a more precise investigation of insulating granular aluminum films, applying magnetic field, which offers a selective way to manipulate trapped quasiparticles [61], measurements with a fast electric field as presented in Ref. [53], or cold-grown granular aluminum films, which have a slightly different grain size distribution [75].

The authors thank M. Feigel'man, J. Cole, and M. Schechter for helpful discussions and L. Radtke for technical support. Samples were fabricated in the KIT Nanostructure Service Laboratory (NSL). This work was supported by the German Federal Ministry of Education and Research (GeQCoS). The authors acknowledge partial support from the Landesgraduiertenförderung of the state Baden-Württemberg (M.W.) and the Helmholtz International Research School for Teratronics (J.N.V.).

* rotzinger@kit.edu

[1] B. Abeles, R. W. Cohen, and G. W. Cullen, *Phys. Rev. Lett.* **17**, 632 (1966).
 [2] I. S. Beloborodov, A. V. Lopatin, V. M. Vinokur, and K. B. Efetov, *Rev. Mod. Phys.* **79**, 469 (2007).

[3] P. K. Day, H. G. LeDuc, B. A. Mazin, A. Vayonakis, and J. Zmuidzinas, *Nature (London)* **425**, 817 (2003).
 [4] A. Monfardini *et al.*, *Astrophys. J. Suppl. Ser.* **194**, 24 (2011).
 [5] F. Valenti, F. Henriques, G. Catelani, N. Maleeva, L. Grünhaupt, U. von Lüpke, S. T. Skacel, P. Winkel, A. Bilmes, A. V. Ustinov, J. Goupy, M. Calvo, A. Benoît, F. Levy-Bertrand, A. Monfardini, and I. M. Pop, *Phys. Rev. Appl.* **11**, 054087 (2019).
 [6] L. Grünhaupt, M. Spiecker, D. Gusenkova, N. Maleeva, S. T. Skacel, I. Takmakov, F. Valenti, P. Winkel, H. Rotzinger, W. Wernsdorfer, A. V. Ustinov, and I. M. Pop, *Nat. Mater.* **18**, 816 (2019).
 [7] Y. Schön, J. N. Voss, M. Wildermuth, A. Schneider, S. T. Skacel, M. P. Weides, J. H. Cole, H. Rotzinger, and A. V. Ustinov, *npj Quantum Mater.* **5**, 1 (2020).
 [8] D. Rieger, S. Günzler, M. Spiecker, P. Paluch, P. Winkel, L. Hahn, J. K. Hohmann, A. Bacher, W. Wernsdorfer, and I. M. Pop, *Nat. Mater.* **22**, 194 (2022).
 [9] T. T. Hongisto and A. B. Zorin, *Phys. Rev. Lett.* **108**, 097001 (2012).
 [10] J. N. Voss, Y. Schön, M. Wildermuth, D. Dorer, J. H. Cole, H. Rotzinger, and A. V. Ustinov, *ACS Nano* **15**, 4108 (2021).
 [11] N. Samkharadze, A. Bruno, P. Scarlino, G. Zheng, D. P. DiVincenzo, L. DiCarlo, and L. M. K. Vandersypen, *Phys. Rev. Appl.* **5**, 044004 (2016).
 [12] H. Rotzinger, S. T. Skacel, M. Pfirrmann, J. N. Voss, J. Münzberg, S. Probst, P. Bushev, M. P. Weides, A. V. Ustinov, and J. E. Mooij, *Supercond. Sci. Technol.* **30**, 025002 (2017).
 [13] L. Grünhaupt, N. Maleeva, S. T. Skacel, M. Calvo, F. Levy-Bertrand, A. V. Ustinov, H. Rotzinger, A. Monfardini, G. Catelani, and I. M. Pop, *Phys. Rev. Lett.* **121**, 117001 (2018).
 [14] K. Borisov, D. Rieger, P. Winkel, F. Henriques, F. Valenti, A. Ionita, M. Wessbecher, M. Spiecker, D. Gusenkova, I. M. Pop, and W. Wernsdorfer, *Appl. Phys. Lett.* **117**, 120502 (2020).
 [15] Q. He, P. OuYang, M. Dai, H. Guan, J. Hu, S. He, Y. Wang, and L. F. Wei, *AIP Adv.* **11**, 065204 (2021).
 [16] C. Müller, J. H. Cole, and J. Lisenfeld, *Rep. Prog. Phys.* **82**, 31 (2019).
 [17] R. W. Simmonds, K. M. Lang, D. A. Hite, S. Nam, D. P. Pappas, and J. M. Martinis, *Phys. Rev. Lett.* **93**, 077003 (2004).
 [18] G. J. Grabovskij, T. Peichl, J. Lisenfeld, G. Weiss, and A. V. Ustinov, *Science (N.Y.)* **338**, 232 (2012).
 [19] J. Lisenfeld, G. J. Grabovskij, C. Müller, J. H. Cole, G. Weiss, and A. V. Ustinov, *Nat. Commun.* **6**, 6182 (2015).
 [20] J. Lisenfeld, A. Bilmes, S. Matiyahu, S. Zanker, M. Marthaler, M. Schechter, G. Schön, A. Shnirman, G. Weiss, and A. V. Ustinov, *Sci. Rep.* **6**, 23786 (2016).
 [21] S. Matiyahu, J. Lisenfeld, A. Bilmes, A. Shnirman, G. Weiss, A. V. Ustinov, and M. Schechter, *Phys. Rev. B* **95**, 241409(R) (2017).
 [22] A. Bilmes, S. Volosheniuk, J. D. Brehm, A. V. Ustinov, and J. Lisenfeld, *npj Quantum Inf.* **7**, 1 (2021).
 [23] B. Sarabi, A. N. Ramanayaka, A. L. Burin, F. C. Wellstood, and K. D. Osborn, *Appl. Phys. Lett.* **106**, 172601 (2015).

- [24] J. D. Brehm, A. Bilmes, G. Weiss, A. V. Ustinov, and J. Lisenfeld, *Appl. Phys. Lett.* **111**, 112601 (2017).
- [25] J. Gao, J. Zmuidzinas, B. A. Mazin, H. G. LeDuc, and P. K. Day, *Appl. Phys. Lett.* **90**, 102507 (2007).
- [26] D. P. Pappas, M. R. Vissers, D. S. Wisbey, J. S. Kline, and J. Gao, *IEEE Trans. Appl. Supercond.* **21**, 871 (2011).
- [27] J. Burnett, L. Faoro, I. Wisby, V. L. Gurtovoi, A. V. Chernykh, G. M. Mikhailov, V. A. Tulin, R. Shaikhaidarov, V. Antonov, P. J. Meeson, A. Y. Tzalenchuk, and T. Lindström, *Nat. Commun.* **5**, 4119 (2014).
- [28] J. Goetz, F. Deppe, M. Haerberlein, F. Wulschner, C. W. Zollitsch, S. Meier, M. Fischer, P. Eder, E. Xie, K. G. Fedorov, E. P. Menzel, A. Marx, and R. Gross, *J. Appl. Phys.* **119**, 015304 (2016).
- [29] D. Niepce, J. J. Burnett, M. G. Latorre, and J. Bylander, *Supercond. Sci. Technol.* **33**, 025013 (2020).
- [30] G. Deutscher, H. Fenichel, M. Gershenson, E. Grünbaum, and Z. Ovadyahu, *J. Low Temp. Phys.* **10**, 231 (1973).
- [31] M. Wildermuth, L. Powalla, J. N. Voss, Y. Schön, A. Schneider, M. V. Fistul, H. Rotzinger, and A. V. Ustinov, *Appl. Phys. Lett.* **120**, 112601 (2022).
- [32] J. Lisenfeld, A. Bilmes, A. Megrant, R. Barends, J. Kelly, P. Klimov, G. Weiss, J. M. Martinis, and A. V. Ustinov, *npj Quantum Inf.* **5**, 1 (2019).
- [33] See Supplemental Material at <http://link.aps.org/supplemental/10.1103/PhysRevLett.132.217002>, which includes Refs. [34–37], for details on the experimental setup, sample fabrication, electric field simulations, resonator properties and TLS statistics as well as additional measurement data.
- [34] T. Koyama, *Phys. Rev. B* **70**, 226503 (2004).
- [35] G. Deutscher, *J. Supercond. Novel Magn.* **34**, 1699 (2021).
- [36] B. Bandyopadhyay, P. Lindenfeld, W. L. McLean, and H. K. Sin, *Phys. Rev. B* **26**, 3476 (1982).
- [37] M. Devoret, S. Girvin, and R. Schoelkopf, *Ann. Phys. (Berlin)* **519**, 767 (2007).
- [38] A. Schneider, Quantum sensing experiments with superconducting qubits, Ph.D. thesis, Karlsruhe Institute of Technology, 2020.
- [39] Y. Shalibo, Y. Rofe, D. Shwa, F. Zeides, M. Neeley, J. M. Martinis, and N. Katz, *Phys. Rev. Lett.* **105**, 177001 (2010).
- [40] L. Faoro and L. B. Ioffe, *Phys. Rev. B* **91**, 014201 (2015).
- [41] C. Müller, J. Lisenfeld, A. Shnirman, and S. Poletto, *Phys. Rev. B* **92**, 035442 (2015).
- [42] S. Schlör, J. Lisenfeld, C. Müller, A. Bilmes, A. Schneider, D. P. Pappas, A. V. Ustinov, and M. Weides, *Phys. Rev. Lett.* **123**, 190502 (2019).
- [43] L. Faoro and L. B. Ioffe, *Phys. Rev. Lett.* **109**, 157005 (2012).
- [44] P. W. Anderson, B. I. Halperin, and C. M. Varma, *J. Appl. Phys.* **25**, 1 (1972).
- [45] W. A. Phillips, *J. Low Temp. Phys.* **7**, 351 (1972).
- [46] M. S. Khalil, M. J. A. Stoutimore, F. C. Wellstood, and K. D. Osborn, *J. Appl. Phys.* **111**, 054510 (2012).
- [47] B. Sarabi, Cavity quantum electrodynamics of nanoscale two-level systems, Ph.D. thesis, University of Maryland, 2014.
- [48] M. Von Schickfus and S. Hunklinger, *Phys. Lett.* **64A**, 144 (1977).
- [49] B. Golding, M. v. Schickfus, S. Hunklinger, and K. Dransfeld, *Phys. Rev. Lett.* **43**, 1817 (1979).
- [50] J. M. Martinis, K. B. Cooper, R. McDermott, M. Steffen, M. Ansmann, K. D. Osborn, K. Cicak, S. Oh, D. P. Pappas, R. W. Simmonds, and C. C. Yu, *Phys. Rev. Lett.* **95**, 210503 (2005).
- [51] B. Sarabi, A. N. Ramanayaka, A. L. Burin, F. C. Wellstood, and K. D. Osborn, *Phys. Rev. Lett.* **116**, 167002 (2016).
- [52] A. Bilmes, A. Megrant, P. Klimov, G. Weiss, J. M. Martinis, A. V. Ustinov, and J. Lisenfeld, *Sci. Rep.* **10**, 3090 (2020).
- [53] L. Yu, S. Matityahu, Y. J. Rosen, C.-C. Hung, A. Maksymov, A. L. Burin, M. Schechter, and K. D. Osborn, *Sci. Rep.* **12**, 16960 (2022).
- [54] M. Schechter and P. C. E. Stamp, *Phys. Rev. B* **88**, 174202 (2013).
- [55] A. L. Efros and B. I. Shklovskii, *J. Phys. C* **8**, L49 (1975).
- [56] A. Churkin, D. Barash, and M. Schechter, *Phys. Rev. B* **89**, 104202 (2014).
- [57] M. Sidorova, A. D. Semenov, H. W. Hübers, S. Gyger, and S. Steinhauer, *Supercond. Sci. Technol.* **35**, 105005 (2022).
- [58] V. Lubchenko and P. G. Wolynes, *Phys. Rev. Lett.* **87**, 195901 (2001).
- [59] F. Levy-Bertrand, T. Klein, T. Grenet, O. Dupré, A. Benoît, A. Bideaud, O. Bourrion, M. Calvo, A. Catalano, A. Gomez, J. Goupy, L. Grünhaupt, U. V. Luepke, N. Maleeva, F. Valenti, I. M. Pop, and A. Monfardini, *Phys. Rev. B* **99**, 094506 (2019).
- [60] M. Kristen, J. N. Voss, M. Wildermuth, H. Rotzinger, and A. V. Ustinov, *Appl. Phys. Lett.* **122**, 202602 (2023).
- [61] S. E. de Graaf, L. Faoro, L. B. Ioffe, S. Mahashabde, J. J. Burnett, T. Lindström, S. E. Kubatkin, A. V. Danilov, and A. Y. Tzalenchuk, *Sci. Adv.* **6**, eabc5055 (2020).
- [62] N. Bachar, S. Lerer, A. Levy, S. Hacozen-Gourgy, B. Almog, H. Saadaoui, Z. Salman, E. Morenzoni, and G. Deutscher, *Phys. Rev. B* **91**, 041123(R) (2015).
- [63] F. Yang, T. Gozlinski, T. Storbeck, L. Grünhaupt, I. M. Pop, and W. Wulfhekkel, *Phys. Rev. B* **102**, 104502 (2020).
- [64] K. B. Efetov, *Sov. Phys. JETP* **51** (1980).
- [65] U. S. Pracht, N. Bachar, L. Benfatto, G. Deutscher, E. Farber, M. Dressel, and M. Scheffler, *Phys. Rev. B* **93**, 100503(R) (2016).
- [66] V. Humbert, M. Ortuño, A. M. Somoza, L. Bergé, L. Dumoulin, and C. A. Marrache-Kikuchi, *Nat. Commun.* **12**, 1 (2021).
- [67] R. H. Koch, D. P. DiVincenzo, and J. Clarke, *Phys. Rev. Lett.* **98**, 267003 (2007).
- [68] R. M. Lutchyn, L. Cywinski, C. P. Nave, and S. Das Sarma, *Phys. Rev. B* **78**, 024508 (2008).
- [69] J. Burnett, L. Faoro, and T. Lindström, *Supercond. Sci. Technol.* **29**, 044008 (2016).
- [70] K. Agarwal, I. Martin, M. D. Lukin, and E. Demler, *Phys. Rev. B* **87**, 144201 (2013).
- [71] S. Chakravarty, S. Kivelson, G. T. Zimanyi, and B. I. Halperin, *Phys. Rev. B* **35**, 7256 (1987).
- [72] P. Raychaudhuri and S. Dutta, *J. Phys. Condens. Matter* **34**, 083001 (2021).
- [73] A. V. Khvalyuk, T. Charpentier, N. Roch, B. Sacépé, and M. V. Feigel'man, *arXiv:2311.15126*.
- [74] U. S. Pracht, T. Cea, N. Bachar, G. Deutscher, E. Farber, M. Dressel, M. Scheffler, C. Castellani, A. M. García-García, and L. Benfatto, *Phys. Rev. B* **96**, 094514 (2017).
- [75] G. Deutscher, M. Gershenson, E. Grünbaum, and Y. Imry, *J. Vac. Sci. Technol.* **10**, 697 (1973).